Article

Domain Separated Density Functional Theory for Reaction Energy Barriers and Optical Excitations

Published as part of The Journal of Physical Chemistry virtual special issue "Peter J. Rossky Festschrift".

Martín A. Mosquera, Leighton O. Jones, Carlos H. Borca, Mark A. Ratner, and George C. Schatz*

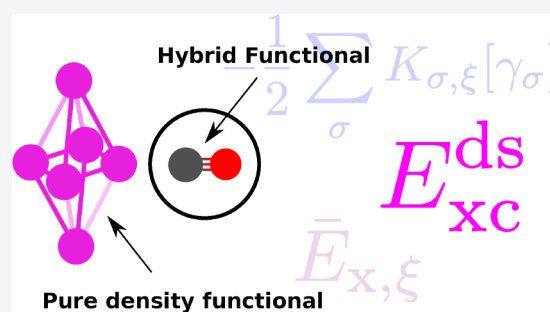Cite This: *J. Phys. Chem. A* 2020, 124, 5954−5962

Read Online

ACCESS | Metrics & More | Article Recommendations | Supporting Information

ABSTRACT: We recently proposed domain separated density functional theory (DS-DFT), a framework that allows for the combination of different levels of theory for the computation of the electronic structure of molecules. This work discusses the application of DS-DFT to the computation of transition-state energy barriers and optical absorption spectra. We considered several hydrogen abstraction reactions and optical spectra of molecule/metal cluster systems, including the absorption of individual species such as carbon monoxide, methane, and molecular hydrogen to a Li_6 cluster. We present and discuss two domain-separated methods: (i), the screened-density approximation (SDA) and (ii) linearly weighted exchange (LWE). We find that SDA, which is applied as a hybridization based on atomic domains, could be useful to computing energy barriers, whereas LWE is suited for the analysis of electronic properties such as ground-state gaps, excitation energies, and oscillator strengths.

$$\frac{1}{2}\sum_{\sigma} K_{\sigma,\xi}[\gamma_\sigma]$$

Hybrid Functional

E^{ds}_{xc}

$\bar{E}_{x,\xi}$

Pure density functional

1. INTRODUCTION

Density functional theory (DFT) methods are widely used in electronic structure studies due to their reliability and computational accessibility. The electronic energy is conveniently calculated by a set of density functionals that capture the relevant physical contributions to it. The most popular type of DFT method is that of hybrid functionals.[1−3] They are commonly used as they provide useful estimation to quantities such as energy gaps, optical excitation energies, reaction energetics, among others, so that they can provide guidance to the understanding of molecular systems. For large molecular architectures, however, the applicability of hybrid functional methods can be quite challenging. This has been a strong motivation to develop quantum embedding (QE) methodologies,[4−6] designed to apply different levels of theory to different parts of a molecule or collection of molecules (dimers, bound systems, etc.), with the goal of achieving both the control of computational cost and the accuracy of a calculation.

Defining the level of theory sometimes requires the user to decide how to treat the exchange and the correlation energies. For example, in standard hybrid functionals, the exchange energy is decomposed into a contribution from Hartree−Fock (HF) exchange and another one from a purely density-dependent (PDD) exchange functional (such as a generalized gradient approximation, or GGA, exchange, for instance). In other cases, such as multi-heavy-metal complexes,[7] the correlation effects need to be described by a wave function based level of theory such as complete active space, or a related

technique. With QE methods, we can assign a region of interest a hybrid functional (or wave function method), and a more efficient methodology to complement such a region of interest; it is assumed of course, that this region necessitates the methodology of higher accuracy.

Domain separated DFT (DS-DFT) is a theory to perform QE calculations as described above. In this theory, a domain (or switching) function is used to separate quantum mechanical operators into those that are to be study with a wave function methodology, and those to be analyzed with density functional theory. We showed, as an example, that HF theory can be combined with DFT, giving physically meaning results.[8] In these calculations, however, the domain function was not employed explicitly. In ref [9], we suggested that density fitting techniques can be employed to simplify the computation of the domain separated (DS) HF exchange contributions. In this work, we apply this idea to the combination of hybrid functionals with PDD ones.

PDD functionals are commonly employed in plane-wave DFT codes to study extended structures such as nanotubes, two-dimensional materials, and semiconducting crystals. On

the other hand, hybrid functionals, which use a component of wave function theory, namely HF exchange (and perturbative correlation, as in the case of double hybrid functionals[10]), often lead to calculation of optoelectronic properties of single molecules, organic or inorganic.[11] For large- or extended-system computations, however, HF exchange (and orbital dependent correlation) can be computationally demanding due to the high number of electronic repulsion integrals that need to be determined to construct the exchange matrix of the system being studied. For this reason, it is important to develop algorithms that combine theories. Figure 1 illustrates a potential application in this direction.
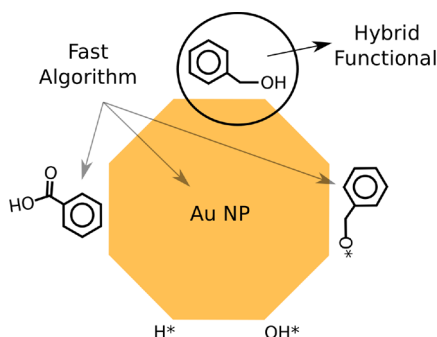

Figure 1. Example of a potential embedding DS-DFT model. For the oxidation of an organic alcohol chemisorbed on the surface of a Au nanoparticle, one could select what molecules could be studied with a hybrid functional and treat the environment with a more computational efficient theory.

In the field of QE, a series of productive theories and methods have been proposed to address different challenges.[12−24] Some of these methods involve the use of an auxiliary operator or mechanism that localizes orbitals within a region of interest, or the use of an embedding self-energy that permits the mixing of different levels of theory. For molecule–solvent interactions, among others, subsystem DFT and frozen-density embedding are established methods to study such types of situations.[12,14] We recently proposed that the idea of range separation in DFT,[25−27] and the generalized Kohn–Sham theory[28] can be employed to combine different levels of electronic structure theories, including description of correlation by wave functions.[8]

In this work we utilize domain separation as a means to further extend the applicability of hybrid functionals. Standard hybrid functionals mix globally fixed amounts of HF exchange and pure DFT exchange. This admixture is applied to the entire space. With domain separation, one can instead control this mixing locally, so a hybrid functional can be applied specifically to a region of interest in the molecule. In addition, we can also apply domain separation atom-wise, adding possibilities for the creation of alternative hybrid functionals. This can be useful to eliminate or reduce adverse effects such as self-interaction errors which are present in regions of low electronic density (near hydrogen atoms, for example). We apply these ideas to the calculation of transition-state energy barriers, and electronic spectra. Two DS XC approximations are explored: the screened-density approximation, and the linearly weighted exchange. These show promising results for the calculation of energetic properties, and may motivate their implementation for large-scale computational studies.

2. THEORY IMPLEMENTATION

In this section, we describe the steps we follow in the implementation of DS-DFT and DS-TDDFT calculations. The formal theoretical background is presented in ref 8, and additional details are discussed in refs 9 and 29.

2.1. Ground State DS-DFT. To motivate the form of XC energy used in this work, we consider the following basic type of hybrid functional:

$$E_{xc}^{hyb}[\{\rho_\sigma\}, \{\gamma_\sigma\}] = aE_x^{HF}[\{\gamma_\sigma\}] + (1 - a)E_x^{DFA}[\{\rho_\sigma\}] + E_c^{DFA}[\{\rho_\sigma\}] \tag{1}$$

Here E_x^{DFA} and E_c^{DFA} are PDD exchange and correlation energies, respectively (these are determined through a density functional approximation, or DFA), and E_x^{HF} is the HF exchange energy; σ and τ label spin. γ_σ denotes the spin-polarized 1-body density matrix:

$$\gamma_\sigma(\mathbf{r}', \mathbf{r}) = \sum_i \varphi_{i\sigma}^*(\mathbf{r}')\varphi_{i\sigma}(\mathbf{r}) \tag{2}$$

Here $\varphi_{i\sigma}$ denotes an occupied molecular orbital, with the energy level i and z-spin σ. The spin electronic density is simply $\rho_\sigma(\mathbf{r}) = \gamma_\sigma(\mathbf{r},\mathbf{r})$. To apply domain separation to this kind of functional, we replace a by a switching function, or domain function, denoted as $\xi(\mathbf{r})$. This function, $\xi(\mathbf{r})$, determines the region where a portion of HF exchange is computed, in this region $\xi \rightarrow \sqrt{a}$; the function tends to zero otherwise (Figure 2). By employing the domain function we can combine a hybrid functional with a pure DFA. In the next two subsections, 2.2 and 2.3, we show different forms of this function that we use.
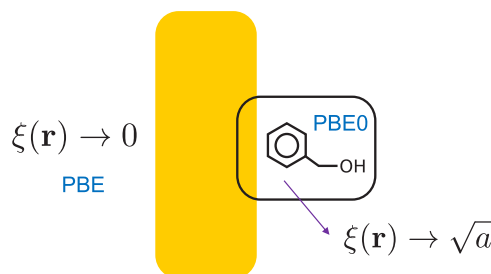

Figure 2. Illustration of domain separation applied to benzyl alcohol adsorbed on a Au surface. In the molecular region $\xi \rightarrow \sqrt{a}$, everywhere else $\xi \rightarrow 0$. We use $\sqrt{a}$ because the domain function appears twice in the definition of $K_{\xi,\sigma}$. If a functional such as PBE (Perdew–Burke–Ernzerhof) were employed for the PDD part, and $a = 1/4$, then with eq 3, we would obtain a spatial combination of PBE0 and PBE.

The above leads to a domain separated XC energy, which in the spin-polarized form reads

$$E_{xc}^{ds}[\{\rho_\tau\}, \{\gamma_\tau\}] = -\frac{1}{2}\sum_\sigma K_{\sigma,\xi}[\{\gamma_\sigma\}] + \bar{E}_{x,\xi}^{DFA}[\{\rho_\tau\}] + E_c^{DFA}[\{\rho_\tau\}] \tag{3}$$

where $K_{\sigma,\xi}$ is the polarized domain-screened HF exchange energy:

$$K_{\sigma,\xi}[\{\gamma_\sigma\}] = \int d^3\mathbf{r}\, d^3\mathbf{r}'\, \xi(\mathbf{r})\xi(\mathbf{r}') \frac{|\gamma_\sigma(\mathbf{r}', \mathbf{r})|^2}{|\mathbf{r} - \mathbf{r}'|} \tag{4}$$

$\overline{E}_{x,\xi}^{DFA}$ is the complementary exchange energy to $-(^{1}/_{2})\sum_{\sigma}K_{\sigma,\xi}$. In regions where $\xi \to 0$, the standard local exchange energy-density contributes $\overline{E}_{x,\xi}^{DFA}$; otherwise, it is partially reduced because of the nonlocal exchange contribution. Determining how to treat the local exchange in the hybrid functional region is the subject of the next two subsections, 2.2 and 2.3.

In analogy with standard HF algorithms, the computation of the domain-screened HF exchange energy can be carried out through an exchange matrix:

$$K_{\sigma,\xi,\mu\nu} = \int d^3\mathbf{r}\, d^3\mathbf{r}'\, \xi(\mathbf{r})\xi(\mathbf{r}')\, \phi_\mu(\mathbf{r})\frac{\gamma_\sigma(\mathbf{r}', \mathbf{r})}{|\mathbf{r} - \mathbf{r}'|}\phi_\nu(\mathbf{r}') \quad (5)$$

where ϕ_μ denotes a basis function. As suggested in ref 9, the above matrix can be computed by means of "orbital" fitting. First, we define the orbital:

$$\varphi_{\xi,i\sigma}(\mathbf{r}) = \xi(\mathbf{r})\varphi_{i\sigma}(\mathbf{r})$$
$$= \sum_\mu C_{\xi,\mu}^{i\sigma}\phi_\mu(\mathbf{r}). \quad (6)$$

By applying the least-squares method to minimize the difference between $\xi(\mathbf{r})\varphi_{i\sigma}(\mathbf{r})$ and $\sum_\mu C_{\xi,\mu}^{i\sigma}\phi_\mu(\mathbf{r})$, we obtain

$$\mathbf{C}_\xi^{i\sigma} = \mathbf{S}^{-1}\mathbf{\Xi}\mathbf{C}^{i\sigma} \quad (7)$$

where $\Xi_{\mu\nu} = \int d^3\mathbf{r}\, \phi_\mu(\mathbf{r})\xi(\mathbf{r})\phi_\nu(\mathbf{r})$, and $\mathbf{C}$ denotes the molecular vectors of the standard molecular orbitals $\varphi_{i\sigma}(\mathbf{r}) = \sum_\mu \mathbf{C}_\mu^{i\sigma}\phi_\mu$. This matrix can be determined using the standard integration grid used in DFT algorithms. With these fitting techniques, the auxiliary density matrix $D_{\sigma,\mu\nu}^\xi = \sum_i C_{\xi,\mu}^{i\sigma}C_{\xi,\nu}^{i\sigma}$ can be employed along with regular electron repulsion integrals.[9]

2.2. Screened Density Approximation. In our previous work, for HF theory/DFA embedding, we employed the approximation to the PDD exchange ($\overline{E}_{x,\xi}^{DFA}$):

$$\overline{E}_{x,\xi}^{sda}[\{\rho_\tau\}] = E_x^{DFA}[\{\rho_\tau\}] - E_x^{DFA}[\{\rho_{\xi,\tau}\}] \quad (8)$$

where

$$\rho_{\xi,\tau}(\mathbf{r}) = \xi^2(\mathbf{r})\rho_\tau(\mathbf{r}) \quad (9)$$

In this work, we refer to the above functional as the "screened-density approximation" (SDA). It consists in the calculations and comparison of the standard exchange energy evaluated at the net and screened spin-density $\xi^2(\mathbf{r})\rho_\sigma(\mathbf{r})$. In ref 8, for HF/LDA embedding, we noted this led to physically meaningful results for the calculation of band gaps and hydrogen dissociation reactions of the methane and ethylene molecules. Here we extend this idea to combine hybrids with PDD XC functionals. Although the SDA can be applied to a single molecular region of the system, here we apply the SDA to assign different atoms in a molecule different amounts of HF exchange. This allows for reducing locally (and as desired) the adverse, electronic self-interaction.

Ideally, a domain function should approximately be a constant in the embedded region, and smoothly tend to zero as the distance from this region is increased. The smooth transition between the plateau and zero facilitates the fitting of orbitals to compute the domain HF exchange. Motivated by this and for simplicity, we thus apply and explore a series of quartic Gaussian functions to define the domain function (at the end of section 4 we mention other possibilities for these functions):

$$\xi(\mathbf{r}) = \sum_N \sqrt{a_N}\, \exp\left[-\frac{1}{2}\left(\frac{\|\mathbf{r} - \mathbf{R}_N\|}{\sigma_N}\right)^4\right] \quad (10)$$

where the sum runs over the atoms of the system. The a_N parameter denotes the amount of hybridization used for atom N, and σ_N defines the radius where the quartic Gaussians transition from the unity to zero. The SDA is examined for the calculation of energy barriers in section 4. We name a functional based on this procedure as SDA-DFA, where DFA = LDA, PBE, etc. The Results and Discussion examine the application of SDA-PBE.

2.3. Linearly Weighted Exchange. The approximation we discussed in the previous subsection does not balance the HF and PDD exchange, i.e., the sum of exchange contributions in the uniform electron gas limit do not add up to 100% Dirac exchange (we further discuss this point in section 4). If it is required to maintain a balance of exchange contributions, we can use the following approximation to the complementary exchange:[29]

$$\overline{E}_x^{lw}[\{\rho_\tau\}] = \int d^3\mathbf{r}\, [1 - \xi^2(\mathbf{r})]e_x^{DFA}(\{y_\tau\})\Big|_{y_\tau = \rho_\tau(\mathbf{r})} \quad (11)$$

Here e_x^{DFA} is the standard, approximated, local exchange energy density. We thus treat the square of ξ as a local weight, and we refer to this approximation as "linearly weighted exchange" (LWE). With this formula, in the limit where the domain function tends to a constant, the sums of the HF and PDD exchange add to 100%. The exchange is thus linearly balanced with respect to ξ.[2] We will study this approximation as applied to the computation of excitation energies.

For the calculations based on the LWE functional, we use a single quartic Gaussian:

$$\xi(\mathbf{r}) = \sqrt{a}\, \exp\left[-\frac{1}{2}\left(\frac{\|\mathbf{r} - \mathbf{R}_C\|}{R_{emb}}\right)^4\right] \quad (12)$$

where $\mathbf{R}_C$ is a vector indicating the center of this domain function, and R_{emb} a radius. For distances longer than R_{emb}, the domain function decays. Figure S4 shows a plot of this function for $a = {}^1/_4$ and $R_{emb} = 1.0$.

2.4. Linear Response DS-TDDFT. The linear response equations are relatively straightforward to obtain. For example, one could follow similar steps as in ref.,[30] the only modification is the screening of the Coulomb interaction potential required to define the exchange potential: instead of using $1/|\mathbf{r} - \mathbf{r}'|$ we use $\xi(\mathbf{r})\xi(\mathbf{r}')/|\mathbf{r} - \mathbf{r}'|$. In the Tamm–Dancoff approximation (TDA), this leads us to the domain separated Casida equation:[31]

$$\mathbf{AX} = \Omega\mathbf{X} \quad (13)$$

where $\mathbf{X}$ is an excitation vector, the $\mathbf{A}$ matrix is given by

$$A_{ai\sigma,bj\tau} = (\epsilon_{a\sigma} - \epsilon_{i\sigma})\delta_{ab}\delta_{ij}\delta_{\sigma\tau} + (ai\sigma|\overline{f}_{Hxc,\sigma\tau}^\xi|jb\tau)$$
$$- (ab\sigma|ji\tau)_\xi\delta_{\sigma\tau} \quad (14)$$

and $\epsilon_{p\sigma}$ is the eigenvalue energy of level $p\sigma$. The letters a, b denote virtual orbitals, and i, j, occupied ones. The interaction integrals are defined as follows:

$$(ab\sigma|ji\tau)_\xi = \int d^3\mathbf{r}\, d^3\mathbf{r}'\, \xi(\mathbf{r})\xi(\mathbf{r}')\varphi_{a\sigma}^*(\mathbf{r}')\frac{\varphi_{b\sigma}(\mathbf{r}')\varphi_{j\tau}^*(\mathbf{r})}{|\mathbf{r}'-\mathbf{r}|}\varphi_{i\tau}(\mathbf{r})$$
(15)

and

$$(ai\sigma|\overline{f}_{\text{Hxc},\sigma\tau}^{\xi}|jb\tau)_\xi$$

$$= \int d^3\mathbf{r}\, d^3\mathbf{r}'\, \varphi_{a\sigma}^*(\mathbf{r}')\varphi_{i\sigma}(\mathbf{r}')\overline{f}_{\text{Hxc},\sigma\tau}^{\xi}(\mathbf{r}',\mathbf{r})\varphi_{j\tau}^*(\mathbf{r})\varphi_{b\tau}(\mathbf{r})$$
(16)

The Hartree-XC kernel is defined by the equation

$$\overline{f}_{\text{Hxc},\sigma\tau}^{\xi}(\mathbf{r}',\mathbf{r}) = \frac{1}{|\mathbf{r}'-\mathbf{r}|} + \frac{\delta\overline{E}_{\text{xc}}^{\text{lw}}}{\delta\rho_\tau(\mathbf{r})\delta\rho_\sigma(\mathbf{r}')}$$
(17)

where $\overline{E}_{\text{xc}}^{\text{lw}}=\overline{E}_{\text{x},\xi}^{\text{DFA}}+E_{\text{c}}^{\text{DFA}}$. Using the LWE approximation, the (partial) XC kernel reads

$$\frac{\delta\overline{E}_{\text{xc}}^{\text{lw}}}{\delta\rho_\tau(\mathbf{r})\delta\rho_\sigma(\mathbf{r}')} = \delta(\mathbf{r}'-\mathbf{r})\{[1-\xi^2(\mathbf{r})]f_{\text{x},\sigma\tau}^{\text{DFA}}(\mathbf{r}',\mathbf{r})$$

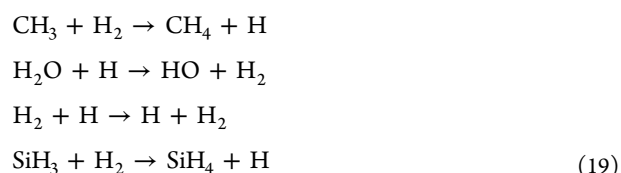$$+ f_{\text{c},\sigma\tau}^{\text{DFA}}(\mathbf{r}',\mathbf{r})\}$$
(18)

where $f_{\text{x},\sigma\tau}^{\text{DFA}}$ and $f_{\text{c},\sigma\tau}^{\text{DFA}}$ are standard (adiabatic) PDD exchange and correlation kernels, correspondingly. The oscillator strengths are calculated as usual by means of the transition dipoles.

3. COMPUTATIONAL METHODOLOGY

To generate reaction paths, we employed the program SIESTA[32,33] and its Lua extension. These paths are determined by the nudged elastic band (NEB) method. The PBE[34] XC functional is used, with the autogenerated numerical Gaussian basis set DZP. An SCF threshold of 1×10^{-7} eV was employed, and 0.03 eV/Å as convergence criterion for the NEB forces. Our calculations use the Python suite PyQuante.[35] We use its algorithms to develop the domain-separated scripts employed to perform the calculations shown in this work. The SDA computations are based on the 6-31G** basis set and applied to the energy barrier calculations. For each barrier calculation, we use the reaction path generated by the SIESTA Lua script. The CCSD(T)[36] calculations were performed with the NWChem[37] program as a reference for the energy barrier estimations, based on the same SIESTA reaction path and basis set (6-31G**, refs 38 and 39). For the LWE DS-TDDFT calculation we also used the mentioned Python code. The basis set for this case is 3-21G (chosen for computational convenience).[40] The XC functional is the local density approximation (LDA). For comparison, we also computed the excitation spectra using configuration interaction singles with doubles perturbative correction, CIS(D),[41] implemented in the program ORCA,[42,43] and same basis set.

4. RESULTS AND DISCUSSION

4.1. Reaction Barriers. Now we consider the computation of the energies of the reactions paths generated with the NEB method. We use five intermediate images for the reactions shown below (more images did not change the barrier significantly):

$$CH_3 + H_2 \rightarrow CH_4 + H$$

$$H_2O + H \rightarrow HO + H_2$$

$$H_2 + H \rightarrow H + H_2$$

$$SiH_3 + H_2 \rightarrow SiH_4 + H$$
(19)

For these reactions, we apply the atom-wise SDA. We assign a domain function to each atom. For hydrogen $a_H = 1.0$ and for the other atoms $a_{\text{Other}} = 0.5$. For each atom σ_N is chosen as its atomic radius (C: 0.7 Å, H: 0.25 Å, O: 0.6 Å, Si: 1.1 Å). Figure 3 shows this embedding scheme for the $H_2O + H$
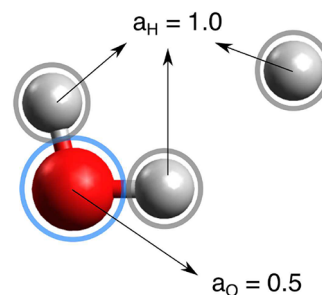

Figure 3. Hybridization based on atomic domains.

reaction. Our rationale for choosing $a_H = 1.0$ for hydrogen is that this reduces the self-interaction error, which is pronounced in regions of low electron-density, such as the hydrogen atoms. We use $a = 0.5$ for C, Si, and O, because it is known that higher amounts of HF exchange around this value are useful to improve transition-state barrier energetics.[44]

Figure 4a shows the results of the first reaction in the series above. A comparison with the functionals PBE[34] and PBE0[2,3] is also displayed in this figure. The PBE functional produces a low barrier, while PBE0 predicts a slightly higher one. The SDA-PBE XC functional improves upon both functionals and yields a barrier closer to that predicted by CCSD(T). The change in energy between products and reagents is also approximately described by SDA-PBE.

For the second reaction, Figure 4b, we also observe that the SDA-PBE curve shows proximity to the reference calculation (and it also shows good agreement for the first NEB step of the calculation, Figure S1). In the other two cases (Figure 4, parts c and d), however, we see mixed results. For $SiH_3 + H_2$, while the height with respect to reagents is well described, it is underestimated for the reverse reaction (due to the over-estimation of the product electronic energy). For the third case ($H_2 + H$), nonetheless, neither PBE0 nor SDA-PBE estimates the reaction barrier properly. However, the domain separation scheme does improve the results with respect to PBE. One potential cause for this behavior is the lack of proper gradient corrections to the density-dependent exchange energy. These corrections should account for the types of atoms involved in the chemical reaction.

Although in the SDA XC functional the HF and PDD exchange contributions do not exactly add up to 100%, we note, however, that the SDA performs in a promising way. The requirement that two functionals add to 100% exchange is needed, for example, in the limit where all the electrons are completely delocalized, as in the uniform electron gas. In molecular systems, this situation is not generally applicable. In such regimes, one could theorize that the form of the exact PDD exchange functional is different from the approximations
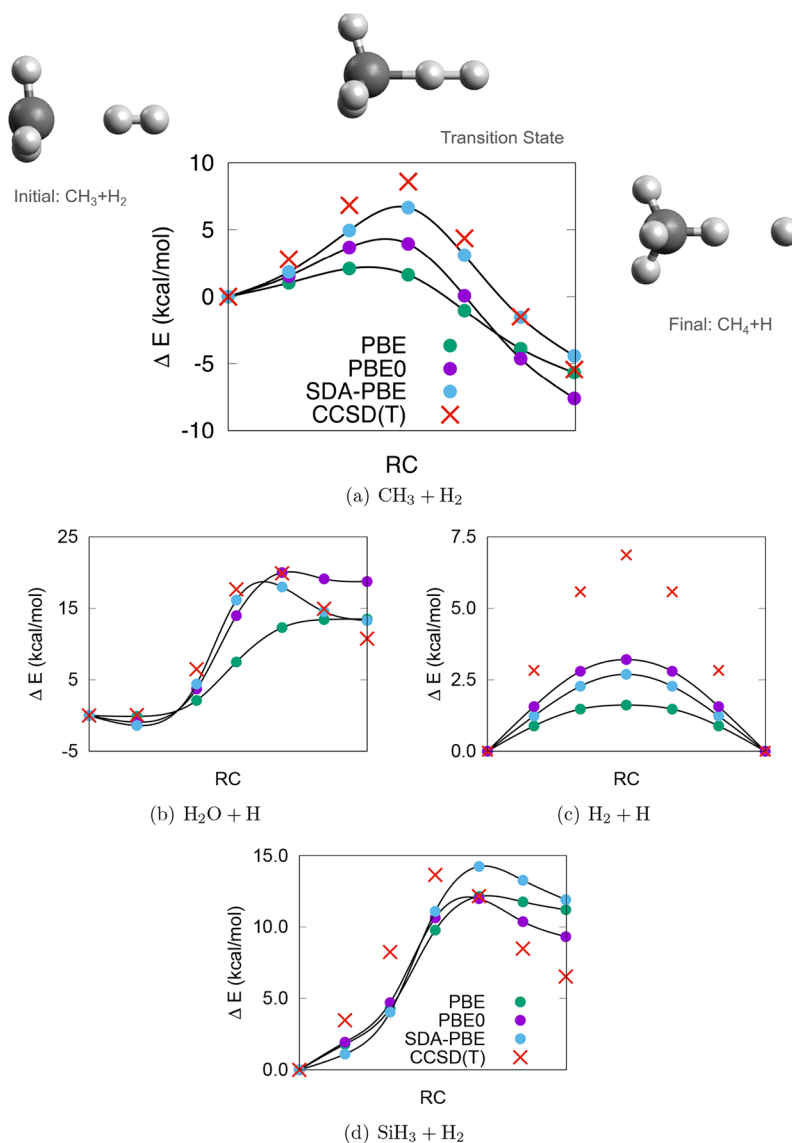
Figure 4. Energy barriers predicted by the SDA, basis set used in all cases is 6-31G**. Matching of colors shown in part c: green, PBE; purple, PBE0; blue, SDA-PBE; cross symbols, CCSD(T). The electronic energy (plus nuclear repulsion) is shown with reference to the reagent configuration (rotational and vibrational contributions are neglected).

we often use. Therefore, that the HF and approximated PDD exchanges add to 100% is a condition that can be relaxed. At the end of the Results and Discussion, we suggest ways to improve the SDA and LWE functional approximations.

The above energy barrier calculations are suggestive of alternative avenues for the estimation of energy properties of molecules. Something we can note is that these calculation only necessitate the domain-screened exchange energy and its purely PDD counterpart; additional energy corrections terms (that are added to the total energy expression) are not required. Furthermore, because the domain functions only modify the Coulombic interaction, in principle, a complete basis set limit can be achieved.

4.2. Excitation Spectra. Now we focus on calculating optical spectra of molecules adsorbed on an octahedral Li_6 cluster. This type of system was studied by Pandey and Schatz[45] in the context of enhanced Raman spectroscopy. The adsorbed molecules are carbon monoxide, methane, and molecular hydrogen. We discuss here mainly the results for

CO, the remaining are reported in the Supporting Information (Figures S5−S10). In this case we locate the domain function ξ around the geometrical center of the molecule, as depicted in Figure 5. The embedding radius is varied from 0 to about 13 Å,
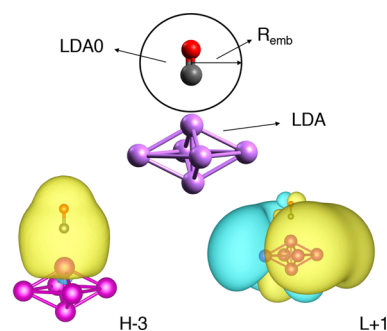

Figure 5. Embedding model for the system CO + Li_6, and molecular orbitals involved in the CT state.

and we set $a = 1/4$ in eq 11. For the sake of simplicity, we apply the LWE, by mixing the XC functionals LDA0[46] and LDA.[47,48] The LDA0 is an XC functional that combines 25% HF exchange with 75% LDA exchange, and 100% LDA correlation. As we reported in ref 46, this functional achieves similar results as PBE0 or B3LYP.[49,50] This is due to the admixing of exchange contribution dominating significantly over the gradient corrections. This trend does not apply to ground-state total energies.[46]

As is well-known, the LDA functional underestimates charge-transfer (CT) excitation energies. This is caused by overdelocalization of the molecular orbitals and overrelaxation of the orbital energies. For the cluster, as electrons are correctly delocalized, a functional such as LDA0 is not required. Therefore, by treating the molecular region with LDA0, and the cluster with LDA, this could lead to improvements in the estimation of CT energies.[51] However, with domain separation, the possibilities for combining different types of XC functionals in general can go beyond LDA0/LDA embedding, as implied before.

In Figure 6 we show the changes in absorption spectrum for different values of R_{emb}, and in the range 6−9 eV. We note that
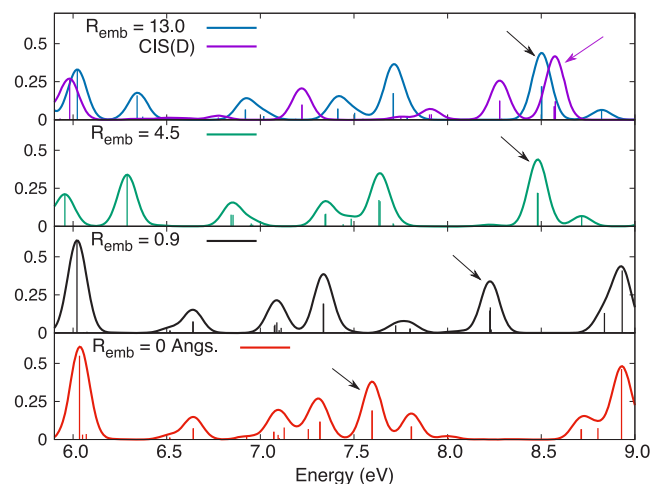

Figure 6. Electronic spectrum (in terms of oscillator strength magnitude (y-axis), which is dimensionless) of CO + Li$_6$ for different values of R_{emb}. Comparison with CIS(D) is shown in the top subplot. Charge-transfer peak is indicated with an arrow. As R_{emb} is increased, the spectrum converges to the LDA0 one.

increasing R_{emb} blue-shifts the CT peak (indicated by arrows) more than the other peaks. As the R_{emb} is increased the CT peak converges toward the peak predicted by CIS(D) (the peak pointed by the arrow in purple color, top subplot in Figure 6), shifting by about 1 eV (this is also observed for CH$_4$ + Li$_6$ and H$_2$ + Li$_6$, Figures S8 and S13). The full dependency of the CT excitation energy as a function of R_{emb} is displayed in Figure 7. With an embedding radius of about 1.3 Å, 99% of the CT energy predicted by LDA0 is obtained. The importance of the inclusion of larger R_{emb} values cannot be overstated, as both excitonic and spin injection have a semidelocalized nature within the basal plane of 2D-functionalized materials.[52]

The CIS(D) calculation also shows a peak at near 6 eV which shows agreement with the LWE calculations, this peak has a strong interband character. However, the LDA0/LDA (or LDA0) bands between this and the CT peak are red-shifted with respect to the CIS(D) results (these have Li s-to-p
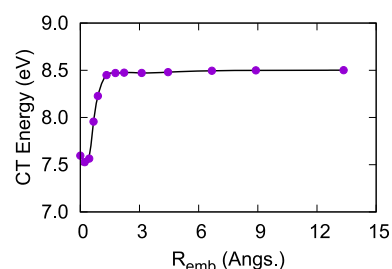

Figure 7. CT excitation energy as a function of R_{emb}. For embedding radii larger than 1.5 Å we note the CT excitation energy converges to the supramolecular LDA0 value.

interband character). This is due to differences in high-energy virtual orbitals with strong lithium p-orbital contributions. In all the cases we studied (Figures 6, 8, S7, S9, S12, and S14) the
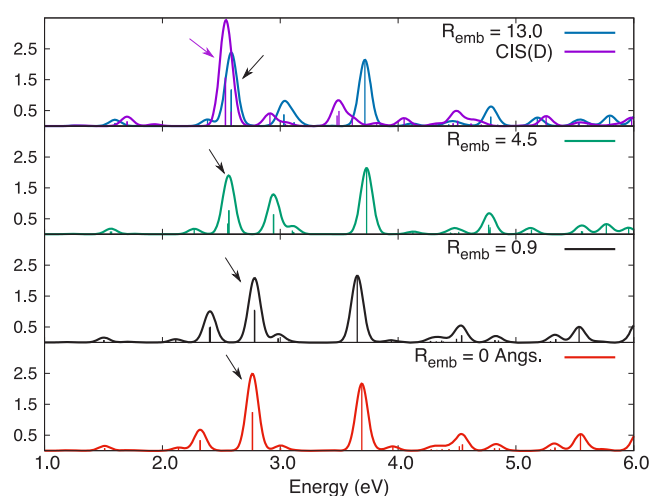

Figure 8. Same as Figure 6, but in range 0−6 eV. The plasmonic peak is indicated with an arrow. Again, as R_{emb} is increased, the spectrum converges to the LDA0 one.

peak heights and positioning may show a nonmonotonic behavior with respect to R_{emb}. However, the peaks become monotonic after R_{emb} is large enough. We attribute the nonmonotonic behavior to fundamental differences between the LDA0 and the LDA XC functionals. Some peaks may not only shift, there can be splitting and changes in their heights. However, all the computed spectra converge from LDA to LDA0 as R_{emb} is increased.

For transitions at lower energies (Figure 8), starting with the pure LDA results, we find the first intense peak (∼2.8 eV) is dominated by s-to-s transitions, so it has a plasmonic character (see also Figure S9 and S14). The second peak around 3.7 eV features "interband" s-to-p character. These peaks show a weak contribution from the CO molecular orbitals, which we believe are responsible for the slight changes in the peak positioning as a function of R_{emb}. However, the peak computed with LDA at around 2.3 eV blue-shifts as R_{emb} is increased. In the top subplot this peak is located near 3 eV (first peak after the plasmonic excitation). This blue-shifting is caused by a strong mixing with CO molecular orbitals. The energies of the CO orbitals are raised because of the inclusion of HF exchange. For the other molecule-cluster systems studied in this work (Supporting Information), we noted that the plasmonic peak does not shift significantly as other transitions (the CT peak

for instance). This is due to the delocalized character of the orbitals involved in this excitations. It is intuitive that a hybrid or a pure DFA should yield similar results in regions where electronic delocalization is dominant.

The other method we discussed in this work, SDA, can be used in analogous way as we used the LWE to perform the optical calculations (as in Figure 5, with no atom-dependent exchange). We expect this application would blueshift the spectra slightly more than LWE. However, using SDA would not be the same as LWE LDA0/LDA, but the hybrid contribution in the embedding region would be similar to the LDA0.

4.3. Extended Functionals. Based on the results presented here for the SDA, it is possible that this functional can improve reaction barriers because of the way the exchange energy is treated. Therefore, a potential domain-separated XC functional of interest for future exploration consists in applying different domain functionals to different exchange energy components. For example,

$$E_{xc}^{ds} = -(K_{\xi} + E_{\theta,x}) + E_c \qquad (20)$$

where θ is a different domain function. With a comprehensive set of reference data, one could perform training (either via nonlinear regression or machine learning) to determine suitable domain functions ξ and θ that yield accurate results. An SDA functional developed in this way can also be combined with traditional functionals, so a region of the system is treated with SDA, whereas the "environment" with a GGA, or something related. Another potential area for future development is the derivation of pure DFAs to be used in conjunction with domain-screened exchange. This could lead to improved estimation of energetics and other properties. The principles employed in DS-DFT provide pathways for DFA development.

The LWE method can be applied in an atom-wise fashion as we used the SDA to calculate reaction energy barriers. We noted in preliminary calculations the reaction barriers were not significantly improved. This suggests that modifications to the PDD exchange contributions may be needed (for example, by changing the gradient corrections) to improve such energy barriers.

Finally, in this work we utilized quartic Gaussians to define the domain functions. This function is convenient because it features a plateau and a smooth transition to zero. There is flexibility in exploring alternative domain functions. The embedding radius, for example, can be replaced by a position-dependent analogue to R_{emb} that is determined by the closest atom. If a domain function is selected, the PDD XC contributions may require adjustments so the net DS XC functional so obtained is accurate and fulfills the intended purpose of the electronic structure calculation.

5. CONCLUSION

We examined the application of domain separation to the calculation of excitation energies, oscillator strengths, and reaction-path energetics. The results show promise for the development of computational and theoretical methods based on DS-DFT. For the calculation of transition-state energy barriers, the SDA is an approximation that could be further developed to enable comprehensive prediction of these barriers. The LWE method can be of interest to compute optical spectra, where there is a specific spatial region that should be studied with a hybrid functional. We found that by combining a hybrid with a purely density-dependent functional the charge-transfer excitation can be blue-shifted, which is an important theoretical feature to be understood for the correct modeling of quantum dots, quantum transduction, the charge transport of transistors, bulk heterojunctions, and more.

ASSOCIATED CONTENT

Supporting Information

The Supporting Information is available free of charge at https://pubs.acs.org/doi/10.1021/acs.jpca.0c03596.

> NEB-unrelaxed H_2O + H energy calculation, zero-order charge-transfer energy calculation for CH_4 + Li_5, embedding models, domain function example, molecular orbitals involved in CT of CH_4 + Li_6 and H_2 + Li_6, and absorption spectra of these systems (PDF)

AUTHOR INFORMATION

Corresponding Author

George C. Schatz − *Department of Chemistry, Northwestern University, Evanston, Illinois 60208, United States;* orcid.org/0000-0001-5837-4740; Phone: +1-847-491-5371; Email: g-schatz@northwestern.edu

Authors

Martín A. Mosquera − *Department of Chemistry, Northwestern University, Evanston, Illinois 60208, United States;* orcid.org/0000-0003-2170-5651

Leighton O. Jones − *Department of Chemistry, Northwestern University, Evanston, Illinois 60208, United States;* orcid.org/0000-0001-6657-2632

Carlos H. Borca − *Department of Chemical and Biological Engineering, Princeton University, Princeton, New Jersey 08544, United States;* orcid.org/0000-0003-0683-7613

Mark A. Ratner − *Department of Chemistry, Northwestern University, Evanston, Illinois 60208, United States;* orcid.org/0000-0001-7983-3387

Complete contact information is available at:
https://pubs.acs.org/10.1021/acs.jpca.0c03596

Notes

The authors declare no competing financial interest.

REFERENCES

(1) Becke, A. D. A. New Mixing of Hartree−Fock and Local Density-Functional Theories. *J. Chem. Phys.* **1993**, *98*, 1372−1377.

(2) Perdew, J. P.; Ernzerhof, M.; Burke, K. Rationale for Mixing Exact Exchange with Density Functional Approximations. *J. Chem. Phys.* **1996**, *105*, 9982−9985.

(3) Adamo, C.; Barone, V. Toward Reliable Density Functional Methods without Adjustable Parameters: The PBE0Model. *J. Chem. Phys.* **1999**, *110*, 6158−6170.

(4) Wesolowski, T. A.; Shedge, S.; Zhou, X. Frozen-Density Embedding Strategy for Multilevel Simulations of Electronic Structure. *Chem. Rev.* **2015**, *115*, 5891−5928.

(5) Severo Pereira Gomes, A.; Jacob, C. R. Quantum-Chemical Embedding Methods for Treating Local Electronic Excitations in Complex Chemical Systems. *Annu. Rep. Prog. Chem., Sect. C: Phys. Chem.* **2012**, *108*, 222−277.

(6) Neugebauer, J. Chromophore-Specific Theoretical Spectroscopy: From Subsystem Density Functional Theory to Mode-Specific Vibrational Spectroscopy. *Phys. Rep.* **2010**, *489*, 1−87.

(7) Vlaisavljevich, B.; Andrews, L.; Wang, X.; Gong, Y.; Kushto, G. P.; Bursten, B. E. Detection and Electronic Structure of Naked Actinide Complexes: Rhombic-Ring $(AnN)_2$ Molecules Stabilized by Delocalized π-Bonding. *J. Am. Chem. Soc.* **2016**, *138*, 893−905.

(8) Mosquera, M. A.; Jones, L. O.; Borca, C. H.; Ratner, M. A.; Schatz, G. C. Domain Separation in Density Functional Theory. *J. Phys. Chem. A* **2019**, *123*, 4785−4795.

(9) Mosquera, M. A.; Jones, L. O.; Ratner, M. A.; Schatz, G. C. Quantum Embedding for Material Chemistry Based on Domain Separation and Open Subsystems. *Int. J. Quantum Chem.* **2020**, No. e26184.

(10) Goerigk, L.; Grimme, S. Double-Hybrid Density Functionals. *WIRES Comput. Mol. Sci.* **2014**, *4*, 576−600.

(11) Karton, A.; Tarnopolsky, A.; Lamére, J.-F.; Schatz, G. C.; Martin, J. M. Highly Accurate First-Principles Benchmark Data Sets for the Parametrization and Validation of Density Functional and Other Approximate Methods. Derivation of a Robust, Generally Applicable, Double-Hybrid Functional for Thermochemistry and Thermochemical Kinetics. *J. Phys. Chem. A* **2008**, *112*, 12868−12886.

(12) Cortona, P. Self-Consistently Determined Properties of Solids Without Band-Structure Calculations. *Phys. Rev. B: Condens. Matter Mater. Phys.* **1991**, *44*, 8454.

(13) Georges, A.; Kotliar, G. Hubbard Model in Infinite Dimensions. *Phys. Rev. B: Condens. Matter Mater. Phys.* **1992**, *45*, 6479.

(14) Wesolowski, T. A.; Warshel, A. Frozen Density Functional Approach for Ab Initio Calculations of Solvated Molecules. *J. Phys. Chem.* **1993**, *97*, 8050−8053.

(15) Casida, M. E.; Wesołowski, T. A. Generalization of the Kohn−Sham Equations with Constrained Electron Density Formalism and its Time-Dependent Response Theory Formulation. *Int. J. Quantum Chem.* **2004**, *96*, 577−588.

(16) Elliott, P.; Cohen, M. H.; Wasserman, A.; Burke, K. Density Functional Partition Theory with Fractional Occupations. *J. Chem. Theory Comput.* **2009**, *5*, 827−833.

(17) Huang, C.; Carter, E. A. Potential-Functional Embedding Theory for Molecules and Materials. *J. Chem. Phys.* **2011**, *135*, 194104.

(18) Manby, F. R.; Stella, M.; Goodpaster, J. D.; Miller, T. F., III A Simple, Exact Density-Functional-Theory Embedding Scheme. *J. Chem. Theory Comput.* **2012**, *8*, 2564−2568.

(19) Knizia, G.; Chan, G. K.-L. Density Matrix Embedding: A Simple Alternative to Dynamical Mean-Field Theory. *Phys. Rev. Lett.* **2012**, *109*, 186404.

(20) Fromager, E.; Knecht, S.; Jensen, H. J. A. Multi-Configuration Time-Dependent Density-Functional Theory Based on Range Separation. *J. Chem. Phys.* **2013**, *138*, 084101.

(21) Jacob, C. R.; Neugebauer, J. Subsystem Density-Functional Theory. *WIRES Comput. Mol. Sci.* **2014**, *4*, 325−362.

(22) Akimov, A. V.; Prezhdo, O. V. Large-Scale Computations in Chemistry: A Bird's Eye View of a Vibrant Field. *Chem. Rev.* **2015**, *115*, 5797−5890.

(23) Senjean, B.; Tsuchiizu, M.; Robert, V.; Fromager, E. Local Density Approximation in Site-Occupation Embedding Theory. *Mol. Phys.* **2017**, *115*, 48−62.

(24) Senjean, B.; Nakatani, N.; Tsuchiizu, M.; Fromager, E. Multiple Impurities and Combined Local Density Approximations in Site-Occupation Embedding Theory. *Theor. Chem. Acc.* **2018**, *137*, 169.

(25) Stoll, H.; Savin, A. Density Functionals for Correlation Energies of Atoms and Molecules. *Density Functional Methods In Physics* **1985**, 177−207.

(26) Savin, A. Correlation Contributions from Density Functionals. *Density Functional Methods in Chemistry* **1991**, 213−230.

(27) Leininger, T.; Stoll, H.; Werner, H.-J.; Savin, A. Combining Long-Range Configuration Interaction with Short-Range Density Functionals. *Chem. Phys. Lett.* **1997**, *275*, 151−160.

(28) Seidl, A.; Görling, A.; Vogl, P.; Majewski, J.; Levy, M. Generalized Kohn-Sham Schemes and the Band-Gap Problem. *Phys. Rev. B: Condens. Matter Mater. Phys.* **1996**, *53*, 3764.

(29) Jones, L. O.; Mosquera, M. A.; Schatz, G. C.; Ratner, M. A. Embedding Methods for Quantum Chemistry: Applications from Materials to Life Sciences. *J. Am. Chem. Soc.* **2020**, *142*, 3281−3295.

(30) Mosquera, M. A.; Chen, L. X.; Ratner, M. A.; Schatz, G. C. Sequential Double Excitations from Linear-Response Time-Dependent Density Functional Theory. *J. Chem. Phys.* **2016**, *144*, 204105.

(31) Casida, M. E.; Chong, D. P. Time-Dependent Density Functional Response Theory for Molecules. *Recent Advances in Density Functional Methods, Part I* **1995**, *1*, 155−192.

(32) Artacho, E.; Anglada, E.; Diéguez, O.; Gale, J. D.; García, A.; Junquera, J.; Martin, R. M.; Ordejón, P.; Pruneda, J. M.; Sánchez-Portal, D.; Soler, J. M. The SIESTA Method; Developments and Applicability. *J. Phys.: Condens. Matter* **2008**, *20*, 064208.

(33) Soler, J. M.; Artacho, E.; Gale, J. D.; García, A.; Junquera, J.; Ordejón, P.; Sánchez-Portal, D. The SIESTA Method for Ab Initio Order-N Materials Simulation. *J. Phys.: Condens. Matter* **2002**, *14*, 2745.

(34) Perdew, J. P.; Burke, K.; Ernzerhof, M. Generalized Gradient Approximation Made Simple. *Phys. Rev. Lett.* **1996**, *77*, 3865.

(35) Muller, R. P. *Python Quantum Chemistry (PyQuante) Program*, http://pyquante.sourceforge.net/ 2007,.

(36) Raghavachari, K.; Trucks, G. W.; Pople, J. A.; Head-Gordon, M. A Fifth-Order Perturbation Comparison of Electron Correlation Theories. *Chem. Phys. Lett.* **1989**, *157*, 479−483.

(37) Valiev, M.; Bylaska, E. J.; Govind, N.; Kowalski, K.; Straatsma, T. P.; Van Dam, H. J.; Wang, D.; Nieplocha, J.; Apra, E.; Windus, T. L.; de Jong, W. A. NWChem: A Comprehensive and Scalable Open-Source Solution for Large Scale Molecular Simulations. *Comput. Phys. Commun.* **2010**, *181*, 1477−1489.

(38) Hariharan, P. C.; Pople, J. A. The Influence of Polarization Functions on Molecular Orbital Hydrogenation Energies. *Theor. Chim. Acta* **1973**, *28*, 213−222.

(39) Francl, M. M.; Pietro, W. J.; Hehre, W. J.; Binkley, J. S.; Gordon, M. S.; DeFrees, D. J.; Pople, J. A. Self-Consistent Molecular Orbital Methods. XXIII. A Polarization-Type Basis Set for Second-Row Elements. *J. Chem. Phys.* **1982**, *77*, 3654−3665.

(40) Binkley, J. S.; Pople, J. A.; Hehre, W. J. Self-Consistent Molecular Orbital Methods. 21. Small Split-Valence Basis Sets for First-Row Elements. *J. Am. Chem. Soc.* **1980**, *102*, 939−947.

(41) Head-Gordon, M.; Rico, R. J.; Oumi, M.; Lee, T. J. A Doubles Correction to Electronic Excited States from Configuration Interaction in the Space of Single Substitutions. *Chem. Phys. Lett.* **1994**, *219*, 21−29.

(42) Neese, F. The ORCA Program System. *Wiley Interdiscip. Rev.: Comput. Mol. Sci.* **2012**, *2*, 73−78.

(43) Neese, F. Software Update: The ORCA Program System, version 4.0. *Wiley Interdiscip. Rev.: Comput. Mol. Sci.* **2018**, *8*, No. e1327.

(44) Kang, J. K.; Musgrave, C. B. Prediction of Transition State Barriers and Enthalpies of Reaction by a New Hybrid Density-Functional Approximation. *J. Chem. Phys.* **2001**, *115*, 11040−11051.

(45) Pandey, P. K.; Schatz, G. C. A Detailed Analysis of the Raman Enhancement Mechanisms Associated with the Interaction of a Raman Scatterer with a Resonant Metal Cluster: Results for Li_n-H_2. *J. Chem. Phys.* **1984**, *80*, 2959−2972.

(46) Mosquera, M. A.; Borca, C. H.; Ratner, M. A.; Schatz, G. C. Connection between Hybrid Functionals and Importance of the Local Density Approximation. *J. Phys. Chem. A* **2016**, *120*, 1605−1612.

(47) Dirac, P. A. Note on Exchange Phenomena in the Thomas Atom. *Math. Proc. Cambridge Philos. Soc.* **1930**, *26*, 376−385.

(48) Vosko, S. H.; Wilk, L.; Nusair, M. Accurate Spin-Dependent Electron Liquid Correlation Energies for Local Spin Density Calculations: A Critical Analysis. *Can. J. Phys.* **1980**, *58*, 1200−1211.

(49) Becke, A. Density−Functional Thermochemistry. III. The Role of Exact Exchange. *J. Chem. Phys.* **1993**, *98*, 5648.

(50) Lee, C.; Yang, W.; Parr, R. G. Development of the Colle-Salvetti Correlation-Energy Formula into a Functional of the Electron Density. *Phys. Rev. B: Condens. Matter Mater. Phys.* **1988**, *37*, 785.

(51) Borca, C. H.; Slipchenko, L. V.; Wasserman, A. Ground-State Charge Transfer: Lithium−Benzene and the Role of Hartree−Fock Exchange. *J. Phys. Chem. A* **2016**, *120*, 8190−8198.

(52) Jones, L. O.; Mosquera, M. A.; Ratner, M. A.; Schatz, G. C. Control of Charge Carriers and Band Structure in 2D Monolayer Molybdenum Disulfide via Covalent Functionalization. *ACS Appl. Mater. Interfaces* **2020**, *12*, 4607−4615.